Genetically diverse mouse models of SARS-CoV-2 infection model clinical variation and cytokine responses in COVID-19.

Shelly J Robertson[1], Olivia Bedard[2], Kristin L. McNally[1], Matthew Lewis[1], Chad Clancy[3], Carl Shaia[3], Rebecca M. Broeckel[1], Abhilash I. Chiramel[1], Gail L. Sturdevant[1], Elvira Forte[2], Christoph Preuss[2], Candice N. Baker[2], Daniel E. Sturdevant[4], Craig Martens[4], Steven M. Holland[5], Nadia A. Rosenthal[2,6]* and Sonja M. Best[1]*

[1]Laboratory of Virology, Rocky Mountain Laboratories, National Institute of Allergy and Infectious Diseases, NIH, Hamilton MT USA

[2]The Jackson Laboratory, Bar Harbor Maine USA

[3]Rocky Mountain Veterinary Branch, Rocky Mountain Laboratories, National Institute of Allergy and Infectious Diseases, NIH, Hamilton MT USA

[4]Research Technologies Branch, Rocky Mountain Laboratories, National Institute of Allergy and Infectious Diseases, NIH, Hamilton MT USA

[5]Division of Intramural Research, National Institute of Allergy and Infectious Diseases, NIH, Bethesda MD USA

[6]National Heart and Lung Institute, Imperial College London

*co-corresponding authors

Abstract

Host genetics are a significant determinant of coronavirus disease 2019 (COVID-19)[1]. Animal models that reflect genetic diversity and a range of clinical outcomes observed in human populations are needed to understand mechanisms of severe acute respiratory syndrome coronavirus 2 (SARS-CoV-2) infection dynamics and disease[2]. Here, we report a mouse panel comprising the diverse genetic backgrounds of the Collaborative Cross (CC) founder strains crossed to C57BL/6J mice expressing the K18-hACE2 transgene[3] that enables infection by SARS-CoV-2. Infection of CCxK18-hACE2 F1 progeny resulted in a spectrum of weight loss, survival, viral replication kinetics, histopathology, and cytokine profiles, some of which were sex-specific. Importantly, survival was closely associated with early type I interferon expression and a phased proinflammatory response distinct from mice with severe disease. Thus, dynamics of inflammatory responses observed in COVID-19 can be modeled in diverse mice that provide a genetically tractable platform for understanding antiviral immunity and evaluating countermeasures.

Main

Mice humanized for the main cellular receptor for SARS-CoV-2 entry, angiotensin converting enzyme 2 (ACE2), are valuable pre-clinical infection models[2]. The most widely used model, K18-hACE2, supports high early virus replication in lung epithelial cells, resulting in inflammatory cell infiltration, interstitial edema and focal consolidation of the lung with rapid lethality[4-9]. However, this model on a standard C57BL/6J genetic background does not reflect the wide variety of COVID-19 outcomes in humans, from asymptomatic to severe[10], that are

47 dependent on genetic polymorphisms, age, sex and the presence of underlying conditions[11-13].
48 Multiple studies have demonstrated the value of using genetically diverse mice to assess the
49 impact of host genetics on infectious disease outcomes [14-18]. Indeed, a single genetic background
50 likely will not capture the range of responses and can fail to model key features of disease[19].
51
52 To determine if incorporating genetic diversity could recapitulate the broad phenotypic variation
53 observed in human COVID-19, we crossed the K18-hACE2 strain to the genetically distinct
54 inbred strains A/J, 129S1J, NOD, NZO, PWK, CAST, and WSB that along with C57BL/6J
55 comprise the founders of the Collaborative Cross (CC). This reference population represents
56 90% of the genetic diversity in *M. musculus* populations[20,21] and are used to understand genetic
57 regulation of complex immune responses. Notably, NOD and NZO mice are commonly used in
58 studies of diabetes and metabolic dysfunction that are factors contributing to COVID-19
59 severity[22]. In addition to the 8 CC founder strains, BALB/c and DBA strains were included
60 because BALB/c is widely used in infectious disease modelling, and DBA is a founder strain for
61 BXD strains also used in genetic mapping[23].
62
63 CCxK18-hACE2 F1 mice were infected via intranasal inoculation with 10^3 pfu SARS-CoV-2
64 strain nCoV-WA1-2020 (MN985325.1) and mice were monitored for 21 days. This virus dose is
65 sub-uniformly lethal in the prototype K18-hACE2 strain (C57BL/6J background), resulting in
66 80-90% of mice reaching end-point criteria by 7 days post infection (dpi) (Fig.1). Infection was
67 confirmed by seroconversion to SARS-CoV-2 nucleoprotein in all survivors. Comparative
68 analysis of the eight CCxK18-hACE2 F1 cohorts documented a broad spectrum of weight loss
69 and survival curves characteristic to each CC founder genotype, some of which were sex-specific

70 (Fig. 1). Highly sensitive mice strains included C57BL/6J and A/JxK18-hACE2 that lost
71 approximately 20% of their starting weight between 4 and 7 dpi with no clear sex bias. In
72 contrast, CCxK18-hACE2 F1 progeny from PWK, NZO, 129S1/J (Fig. 1), BALB/c and DBA
73 (Fig. S1) were resistant to clinical disease, generally losing 5-10% starting weight with ~80% of
74 mice surviving infection. Finally, CCxK18-hACE2 F1 progeny of three strains (CAST, NOD,
75 WSB) had marked sexual dimorphism in response, with CAST and NOD F1 males susceptible to
76 lethal disease, although differences in weight loss between sexes were not apparent. Yet another
77 phenotype was obtained in SARS-CoV-2 infected WSB F1 progeny, where infection was
78 uniformly lethal in females. Weight loss in WSB F1 males began later than other groups at 6 dpi
79 and surviving males exhibited sustained weight loss until the end of the observation period in
80 contrast to the rapid weight gain associated with recovery of other CCxK18-hACE2 F1 cohorts.
81
82 In K18-hACE2 mice, SARS-CoV-2 titers peak in the lung at 2-3 dpi and high titers of virus can
83 be isolated from the CNS which may contribute to lethality in this model[24,25]. Thus, virus
84 replication kinetics were determined at 3 and 6 dpi in lung and brain of CCxK18-hACE2 F1
85 cohorts (Fig. 2A, 2B). F1 progeny of sensitive founder strains C57BL/6J and A/J showed high
86 levels of infectious SARS-CoV-2 at 3dpi in lung homogenates that was reduced by 1-2 $\log_{10}$ by 6
87 dpi with no differences between sexes. Infectious virus was generally not recovered from the
88 CNS at 3dpi, but 50% of C57BL/6J and A/J F1 progeny had high virus burden in the CNS by
89 6dpi (10^6-10^8 PFU/g tissue). In contrast, peak lung virus titer in F1 progeny of the most resistant
90 founder strain, PWK, was 150-fold lower than the sensitive strains at 3 dpi and was below the
91 limit of detection at 6dpi. Control of virus replication in PWK F1s was also evident in the CNS
92 where detection of infectious virus was sporadic. Interestingly, F1 progeny of additional CC

93 founder strains classed as resistant had equivalent peak viral titers in the lung to the sensitive
94 K18-hACE2 and A/J F1 progeny, but they tended to control replication by 6 dpi to levels $1\log_{10}$
95 lower than sensitive mice and had less virus burden in the CNS. Finally, lung titers in (CAST,
96 NOD and WSB)xK18-hACE2 F1 progeny were not different between males and females despite
97 differences in clinical severity associated with sex. Thus, F1 progeny of CCxK18-hACE2 mouse
98 strains can be further stratified into a) sensitive F1 progeny with high sustained virus replication
99 in lung and CNS (C57BL/6J, A/J), b) resistant F1 progeny associated with lower peak virus titer
100 and earlier control of replication in the lung with no or low dissemination to other organs (PWK,
101 NZO, 129S1/J), and c) F1 progeny with sex bias where resistance is independent of virus titer in
102 the lung suggesting a sex-based difference in host response (CAST, NOD, WSB). Relative
103 expression of the K18-hACE2 transgene in lung suggested some variability, but expression was
104 not associated with clinical phenotypes or peak viral burden (Fig. S2). Together, these data
105 suggest that the range of clinical severity in mice is only partially associated with control of virus
106 replication (Summarized in Table 1).
107
108 Pathological changes in SARS-CoV-2-infected K18-hACE2 mice were similar to those
109 previously described[7-9,26]. Inflammatory infiltrates evident by 3dpi included perivascular
110 lymphocytes with alveolar septa thickened by neutrophils, macrophages and edema. At 6 dpi,
111 pulmonary pathology was multifocal, and consistent with interstitial pneumonia including type II
112 pneumocyte hyperplasia, septal, alveolar and perivascular inflammation comprised of
113 lymphocytes, macrophages and neutrophils, with alveolar fibrin and edema evident. Bronchiolar
114 pathology was not observed in these mice. Pathology was classified as none, mild (rare scattered
115 inflammatory foci), moderate (coalescing inflammatory foci) or severe (widespread, large

116 inflammatory foci) as exemplified in Fig. 2c. The classification of 'severe' is a comparative term
117 for these mice, as we generally did not observe pathology equivalent to that of the more severe
118 Syrian hamster model of SARS-CoV-2 infection[27-29]. Surprisingly, in comparison to F1 progeny
119 of sensitive founder strains (K18-hACE2 and A/JxK18-hACE2), F1 progeny of resistant PWK,
120 female NZO and 129S/J mice, as well as those of NOD and WSB tended to have higher
121 pathology scores in lungs (Fig. 2d). Lung distribution of viral RNA by RNAscope was limited to
122 type I and II pneumocytes in all strains (Fig. 2b). Pathology in the CNS was scored as present or
123 absent, as it generally consisted of subtle inflammatory foci, including perivascular cuffing and
124 increased gliosis associated with necrotic cells observed in K18-hACE2 and DBAxK18-hACE2
125 F1 males (Fig. S3A-C, G). However, pathology in the CNS of CASTxK18-hACE2 F1 progeny
126 was striking in that microthrombi were evident in capillaries with extensive hemorrhage in the
127 absence of encephalitis, and was associated with viral RNA distribution in the same area (Fig.
128 S3D-F).
129
130 In-depth longitudinal analyses of immune responses in patients with COVID-19 have defined
131 key immunological correlates of disease outcome[30-43]. Moderate COVID-19 is associated with
132 increased plasma levels of a core inflammatory signature of pro-inflammatory cytokines,
133 chemokines and growth factors (e.g., IL-1α, IL-1β, IFNα, IL-12 p70, and IL-17A) that are
134 effectively resolved[43]. In contrast, severe COVID-19 includes sustained expression of these
135 markers with additional signatures including IL-6, IL-10, IL-18, IL-23, TNF-α, and eotaxin
136 among others suggesting that specific timing and failure to resolve inflammatory responses are
137 important factors in disease progression[43]. In SARS-CoV-2-infected CCxK18-hACE2 F1 mice,
138 cytokines and chemokines were quantified in the serum and bronchoalveolar lavage fluid (BAL)

139 by multiplex analysis at 3 and 6 dpi. In general, cytokine levels were much higher in BAL fluid
140 than in serum (Fig. S4A, B; individual data points are provided in Figs. S5-8). Strikingly in the
141 BAL, comparison of sensitive (K18-hACE2 and A/JxK18-hACE2) versus resistant (PWK, NZO
142 and 129S1)xK18-hACE2 F1 progeny revealed that high IFNα expression at 3dpi was associated
143 with survival in both males and females (Fig. 3A, B). Resistant mice also expressed
144 proinflammatory cytokine IL-6, Th1 cytokines (IL-12p70, IL-27) and chemokines (CXCL10,
145 Gro-α/KC, CCL2, CCL3, CCL4, CCL5, CCL7 and CXCL2) (designated as Group A) in BAL at
146 this early timepoint (Fig. 3B, Cluster 1). At 6 dpi, many Group A cytokines were resolving (Fig.
147 3C) while IFN-γ, TNF-α, IL-18, IL-1β, IL-2, IL-4, IL-5, and IL-13 (designated as Group B)
148 were added to the cytokine signature in resistant mice (Fig. 3B, Cluster 2). Interestingly,
149 resistant PWK and NZO x K18-hACE2 mice exhibited a unique profile characterized by
150 tempered levels of Group A and Group B along with high production of IFNγ, Gro-α/KC and
151 eotaxin at 6dpi, a timepoint coincident with the most efficient clearance of virus from the lung
152 (Cluster 4). In contrast, sensitive strains generally failed to produce Group A cytokines at 3 dpi
153 (Cluster 3) and increases in production of Group A and Group B mediators in BAL occurred by
154 6 dpi (Fig. 3B, Cluster 2). Cytokine signatures were less clear in F1 progeny with sex bias
155 (CAST, NOD and WSB) likely due to intermediate survival phenotypes observed in one or both
156 sexes, although responses in BAL were generally higher in males (Fig. S4C). Together, these
157 genetically diverse mice model major dynamic phenotypes observed in human COVID-19.
158 Specifically, reduced disease severity in mice is associated with early type I IFN expression and
159 a phased, controlled inflammatory response. In contrast, a delayed and unorchestrated innate
160 response is associated with lethality.
161

162 Taken together, these observations demonstrate that use of host genetic variation in mice can
163 model different outcomes of SARS-CoV-2 infection, addressing a major deficiency in the toolkit
164 required to combat COVID-19. The phenotypes in diverse mice support a role for the innate
165 immune system in determining COVID-19 severity[32,44-47] and can be used to address key
166 knowledge gaps, including mechanisms of innate immune control of virus replication, defining
167 events needed for a well-orchestrated inflammatory response independent of early viral burden,
168 molecular mechanisms of sex-dependent disease severity, and longer-term implications for tissue
169 repair[48] and lung function.
170

171 **Acknowledgement**

172 This work was funded by the Division of Intramural Research, National Institutes of Health,
173 National Institute of Allergy and Infectious Diseases. Thank you to the animal caretaker staff at
174 campuses of both RML and The Jackson Laboratory for their work in animal husbandry.
175

176 **Declaration of Interests:**

177 The authors have no interests to declare.
178

179 **METHODS**
180

181 Ethics statement
182

183 Animal study protocols were reviewed and approved by the Institutional Animal Care and Use Committee
184 (IACUC) at Rocky Mountain Laboratories (RML), NIAID, NIH in accordance with the recommendations in
185 the Guide for the Care and Use of Laboratory Animals of the NIH. All animal experiments were performed
186 in an animal biosafety level 3 (ABSL3) research facility at RML. Standard operating procedures for work

187 with infectious SARS-CoV-2 and protocols for virus inactivation were approved by the Institutional
188 Biosafety Committee (IBC) and performed under BSL3 conditions.
189
190 Virus preparation
191
192 SARS-CoV-2 (USA_WA1/2020) from University of Texas Medical Branch (Vero passage 4) was
193 propagated on Vero cells cultured in DMEM supplemented with 10% fetal bovine serum, 1 mM L-
194 glutamine, 50U/ml penicillin and 50ug/ml streptomycin. Culture supernatants were collected at 72 hpi,
195 aliquoted and stored at -80ºC.
196
197
198 Mice and virus infection
199
200 CC founder x C57BL/6J -K18-hACE2 F1 were provided by The Jackson Laboratories and include the
201 following: B6.Cg-Tg (K18-ACE2)2PrImn/J), 034860; (A/J x B6.Cg-Tg(K18-ACE2)2PrImn/J)F1/J, 035940;
202 (PWK/PhJ x B6.Cg-Tg(K18-ACE2)2PrImn/J)F1/J, 035938; (NZO/HlLtJ x B6.Cg-Tg(K18-
203 ACE2)2PrImn/J)F1/J, 035936; (129S1/SvImJ x B6.Cg-Tg(K18-ACE2)2PrImn/J)F1/J, 035934; (CAST/EiJ x
204 B6.Cg-Tg(K18-ACE2)2PrImn/J)F1/J, 035937; (NOD/ShiLtJ x B6.Cg-Tg(K18-ACE2)2PrImn/J)F1/J,
205 035935; (WSB/EiJ x B6.Cg-Tg(K18-ACE2)2PrImn/J)F1/J, 035939; (BALB/cJ x B6.Cg-Tg(K18-
206 ACE2)2PrImn/J)F1/J, 035941; (BALB/cJ x B6.Cg-Tg(K18-ACE2)2PrImn/J)F1/J 035943. Six to 12 week-
207 old male and female mice were inoculated by the intranasal route with 10^3 pfu of SARS-CoV-2 in a
208 volume of 50ul PBS (Gibco). Prior to inoculation mice were anesthetized by inhalation of isoflurane.
209 Mice were monitored daily for clinical signs of disease and weight loss.
210
211 Virus titration
212
213 Infectious virus in lung and brain tissue was quantified by plaque assay. Tissues were collected in 0.5ml
214 of DMEM containing 2% FBS, 50U/ml penicillin and 50ug/ml streptomycin and immediately frozen.

215 Tissue samples were weighed, and then homogenized using 5mm steel beads and TissueLyzer II high-
216 speed shaker (Qiagen). Ten-fold serial dilutions of homogenates were prepared in duplicate and used to
217 inoculate Vero cells grown in 48-well tissue culture plates. Following 1 hour incubation at 37ºC, the cells
218 were overlayed with 1.5% carboxymethyl cellulose (CMC) in MEM and incubated at 37ºC for 3-4 days.
219 Cells were then fixed in 10%formalin and plaques were visualized by staining with 1% crystal violet
220 diluted in 10% ethanol.
221
222
223 Measurement of SARS-CoV-2-specific IgG
224
225 Sera were collected at 21 dpi from mice that survived SARS-CoV-2 infection. SARS-CoV-2 spike protein-
226 specific IgG was measured using SARS-CoV2 spike protein serological IgG ELISA kit (Cell Signaling
227 Technology) per manufacturer's instructions.
228
229
230 Multiplex cytokine/chemokine analysis
231
232 Sera were collected from SARS-CoV-2-infected mice at 3 and 6 dpi by centrifugation of whole blood in
233 GelZ serum separation tubes (Sarstedt). BAL samples were recovered by insufflation of lungs with 1 ml
234 sterile PBS followed by aspiration to collect ~0.5ml volume of fluid. SARS-CoV-2 in sera and BAL fluid
235 was inactivated by using γ- irradiation (2 MRad) and removed from the BSL3 laboratory. Cytokine
236 concentrations in serum and BAL were measured using a 26-Procartaplex mouse cytokine/chemokine
237 panel (ThermoFisher EPX260-26088-901) combined with a Simplex IFNα assay (ThermoFisher EPX01A-
238 26027-901). Samples were run on a Luminex Bio-Plex 200 system with BioPlex Manager 6.1.1 software.

239 Histopathology and *in situ* hybridization

240 Tissues were fixed in 10% neutral buffered formalin for a minimum of 7 days with 2 changes according to
241 IBC-approved standard operating procedure. Tissues were processed with a Sakura VIP-6 Tissue Tek,

242 on a 12-hour automated schedule, using a graded series of ethanol, xylene, and PureAffin. Embedded
243 tissues were sectioned at 5 µm and dried overnight at 42°C prior to staining with hematoxylin and
244 eosin. Chromogenic detection of SARS-CoV-2 viral RNA was performed using the RNAscope VS
245 Universal AP assay (Advanced Cell Diagnostics Inc.) on the Ventana Discovery ULTRA stainer using a
246 SARS-CoV-2 specific probe (Advanced Cell Diagnostics Inc. cat#848569). *In situ* hybridization was
247 performed according to manufacturer's instructions.
248
249 Quantitative real-time PCR
250
251 Total lung RNA was extracted from homogenized lysates using the *mir*Vana miRNA Isolation Kit
252 (Invitrogen cat. AM1560) following the manufacturer's protocol for total RNA isolation. Total RNA samples
253 were quantified using a Nanodrop spectrophotometer (Thermo cat. ND-2000C), and reverse transcribed
254 to cDNA using the SuperScript IV VILO Master Mix with ezDNase enzyme (Invitrogen cat. 11766050)
255 following the manufacturer's instructions. Expression of mouse *Ace2*, mouse *Gapdh*, and human ACE2
256 were quantified by qPCR using the ViiA7 Real-Time PCR System (Thermo cat. 44535545). TaqMan
257 probes targeting mouse *Ace2* (Thermo probe ID Mm01159006_m1), mouse *Gapdh* (Thermo probe ID
258 Mm99999915_g1), and human ACE2 (Thermo probe ID Hs01085333_m1) were used in conjunction with
259 the TaqMan Fast Advanced Master Mix (Thermo cat. 4444556) and the ViiA7 Real-Time PCR System
260 with QuantStudio Software (Thermo cat. 44535545). Samples were run in technical triplicate in 10ul
261 reaction volumes on a 384-well plate, and m*Ace2* and hACE2 transcript abundance values were
262 normalized to m*Gapdh* in each sample and relative expression was calculated using a common reference
263 lung sample (C57BL/6J male) and the delta delta-Ct method.
264
265 Statistical analysis
266
267 Comparison of survival curves in males versus females for each strain was performed using the log-rank
268 (Mantel-Cox) test. One-way analysis of variance (ANOVA) with Tukey's multiple comparison posttest was
269 used to compare cytokine and chemokine levels of BAL and serum. Differences between groups were

270 considered significant at a *P* value of <0.05. All statistical analyses were performed with graphPad Prism
271 8.0 (GraphPad Software) or Qlucore Omics Explorer Version 3.7 (Qlucore AB).
272
273 **Figure Legends:**
274
275 **Figure 1: CCxK18-hACE2 F1 progeny mice demonstrate a range of clinical severity**
276 **following infection with SARS-CoV-2.** Mice were infected intranasally with 10^3PFU of SARS-
277 CoV-2 and monitored for survival and weight loss. F1 founder strains were classified as: **a,**
278 sensitive with 50% or greater mortality and no difference between males and females, **b,** resistant
279 with 35% or less mortality, or **c,** sensitive with a sex bias as having statistically significant
280 difference between sensitivity of male and female mice. Mice without evidence of
281 seroconversion at the end of the study were removed from analysis (N=6-8/per sex).
282
283 **Figure 2: Virus replication kinetics and pathology in CCxK18-hACE2 F1 progeny. a,** Virus
284 titers (PFU/g tissue) in lung and brain of male and female mice were measured at 3 and 6 dpi. **b,**
285 RNAscope of SARS-CoV-2 genome predominantly localizing to pneumocytes in areas of lung
286 inflammation. Serial sections demonstrate pathology (upper) and viral RNA distribution (lower;
287 Red). Scale bars represent 100μm. **c,** Examples of pathology scoring used in this study. Scale
288 bars represent 500μm. **d,** Lung pathology scores for CC Founder F1 males and females at 3 and
289 6 dpi. N = 6/time point/sex. ND, not determined.
290
291 **Figure 3: Timing of type I IFN and inflammatory cytokine responses in the lung is**
292 **associated with clinical severity in CCxK18-hACE2 F1 progeny. a,** IFNα protein in BAL

293 from resistant and sensitive mice. **b,** cytokine and chemokine responses in BAL at 3 and 6 dpi. **c,**
294 Resolving group A cytokines in mice resistant to lethality, but not sensitive mice.
295
296
297 **Supplemental Figure 1: Survival, weight loss and SARS-CoV-2 replication kinetics in**
298 **BALB/cxK18-hACE2 or DBAxK18-hACE2 F1 progeny. a,** Survival and weight loss in
299 BALB/cxK18-hACE2 F1. **b,** Survival and weight loss in DBA x K18-hACE2 F1. **c,** Virus titers
300 (PFU/g tissue) in lung and brain of male and female mice were measured at 3 and 6 dpi. **d,**
301 Cytokine expression in BAL.
302
303 **Supplemental Figure 2: Relative expression of human *ACE2* in CCxK18-hACE2 F1**
304 **progeny.** Gene expression was measured by real-time RT-PCR and expressed relative to that in
305 K18-hACE2 mice.
306
307
308 **Supplemental Figure 3: Examples of pathology in the brain of SARS-CoV-2-infected**
309 **CCxK18-hACE2 F1 progeny. a,** Small focal areas of inflammation were most commonly
310 observed (circled). Scale bar = 1000μm. **b,** increased magnification of a. demonstrating
311 perivascular cuffing, gliosis, and evidence of necrotic cells in areas of focal inflammation. Scale
312 bar = 200μm. **c,** Example of a pronounced lymphocytic inflammatory response with perivascular
313 cuffing and increased cellularity (arrowheads). Scale bar = 100μm. **d,** Microthrombus occluding
314 cerebral capillaries and hemorrhage (arrow) observed in CASTxK18-hACE2. Scale bar =
315 100μm. **e,** Example of extensive hemorrhage in the brain of CASTxK18-hACE2 F1 progeny

316 associated with extensive virus replication as demonstrated in f. Scale bar = 1000µm. **f,** serial
317 section relative to e. showing extensive SARS-CoV-2 genome by RNAscope. Scale bar =
318 1000µm. **g,** Incidence of encephalitis for CC Founder F1 males and females at 3 and 6 dpi. ND,
319 not determined.
320
321 **Supplemental Figure 4: Interferon, cytokine and chemokine expression in the serum**
322 **compared to the BAL of SARS-CoV-2-infected female CCxK18-hACE2 F1 progeny.**
323 Cytokines were measured at 3 and 6 dpi by bioplex. **a,** 3 dpi, and **b,** 6dpi for sensitive and
324 resistant strains with no sex-bias. **c,** 3 and 6 dpi from strains with a sex-bias.
325
326 **Supplemental Figure 5: Interferon, cytokine and chemokine expression in the**
327 **bronchoalveolar lavage from SARS-CoV-2-infected male CCxK18-hACE2 F1 progeny.**
328 Cytokines were measured at 3 and 6 dpi by bioplex. The average cytokine expression in BAL of
329 naïve mice is indicated by a grey dashed line.
330
331 **Supplemental Figure 6: Interferon, cytokine and chemokine expression in the serum of**
332 **SARS-CoV-2-infected male CCxK18-hACE2 F1 progeny.** Cytokines were measured at 3 and
333 6 dpi by bioplex. The average cytokine expression in serum of naïve mice is indicated by a grey
334 dashed line.
335
336 **Supplemental Figure 7: Interferon, cytokine and chemokine expression in the**
337 **bronchoalveolar lavage from SARS-CoV-2-infected female CCxK18-hACE2 F1 progeny.**

338 Cytokines were measured at 3 and 6 dpi by bioplex. The average cytokine expression in BAL of
339 naïve mice is indicated by a grey dashed line.
340
341 **Supplemental Figure 8: Interferon, cytokine and chemokine expression in the serum of**
342 **SARS-CoV-2-infected female CCxK18-hACE2 F1 progeny.** Cytokines were measured at 3
343 and 6 dpi by bioplex. The average cytokine expression in serum of naïve mice is indicated by a
344 grey dashed line.
345
346
347 References:

348 1 Severe Covid, G. G. *et al.* Genomewide Association Study of Severe Covid-19 with
349 Respiratory Failure. *N Engl J Med* **383**, 1522-1534, doi:10.1056/NEJMoa2020283 (2020).
350 2 Munoz-Fontela, C. *et al.* Animal models for COVID-19. *Nature* **586**, 509-515,
351 doi:10.1038/s41586-020-2787-6 (2020).
352 3 McCray, P. B., Jr. *et al.* Lethal infection of K18-hACE2 mice infected with severe acute
353 respiratory syndrome coronavirus. *J Virol* **81**, 813-821, doi:10.1128/JVI.02012-06 (2007).
354 4 Chen, R. E. *et al.* In vivo monoclonal antibody efficacy against SARS-CoV-2 variant
355 strains. *Nature* **596**, 103-108, doi:10.1038/s41586-021-03720-y (2021).
356 5 Johnson, B. A. *et al.* Loss of furin cleavage site attenuates SARS-CoV-2 pathogenesis.
357 *Nature* **591**, 293-299, doi:10.1038/s41586-021-03237-4 (2021).
358 6 VanBlargan, L. *et al.* A potently neutralizing anti-SARS-CoV-2 antibody inhibits variants of
359 concern by binding a highly conserved epitope. *bioRxiv*, doi:10.1101/2021.04.26.441501
360 (2021).
361 7 Winkler, E. S. *et al.* SARS-CoV-2 infection of human ACE2-transgenic mice causes severe
362 lung inflammation and impaired function. *Nat Immunol* **21**, 1327-1335,
363 doi:10.1038/s41590-020-0778-2 (2020).
364 8 Yinda, C. K. *et al.* K18-hACE2 mice develop respiratory disease resembling severe COVID-
365 19. *PLoS Pathog* **17**, e1009195, doi:10.1371/journal.ppat.1009195 (2021).
366 9 Zheng, J. *et al.* COVID-19 treatments and pathogenesis including anosmia in K18-hACE2
367 mice. *Nature* **589**, 603-607, doi:10.1038/s41586-020-2943-z (2021).
368 10 Long, Q. X. *et al.* Clinical and immunological assessment of asymptomatic SARS-CoV-2
369 infections. *Nat Med* **26**, 1200-1204, doi:10.1038/s41591-020-0965-6 (2020).
370 11 Docherty, A. B. *et al.* Features of 20 133 UK patients in hospital with covid-19 using the
371 ISARIC WHO Clinical Characterisation Protocol: prospective observational cohort study.
372 *BMJ* **369**, m1985, doi:10.1136/bmj.m1985 (2020).

373 12 Richardson, S. *et al.* Presenting Characteristics, Comorbidities, and Outcomes Among
374 5700 Patients Hospitalized With COVID-19 in the New York City Area. *JAMA* **323**, 2052-
375 2059, doi:10.1001/jama.2020.6775 (2020).
376 13 Pairo-Castineira, E. *et al.* Genetic mechanisms of critical illness in COVID-19. *Nature* **591**,
377 92-98, doi:10.1038/s41586-020-03065-y (2021).
378 14 Graham, J. B. *et al.* Genetic diversity in the collaborative cross model recapitulates
379 human West Nile virus disease outcomes. *mBio* **6**, e00493-00415,
380 doi:10.1128/mBio.00493-15 (2015).
381 15 Gralinski, L. E. *et al.* Genome Wide Identification of SARS-CoV Susceptibility Loci Using
382 the Collaborative Cross. *PLoS Genet* **11**, e1005504, doi:10.1371/journal.pgen.1005504
383 (2015).
384 16 Martin, M. D., Sompallae, R., Winborn, C. S., Harty, J. T. & Badovinac, V. P. Diverse CD8 T
385 Cell Responses to Viral Infection Revealed by the Collaborative Cross. *Cell Rep* **31**,
386 107508, doi:10.1016/j.celrep.2020.03.072 (2020).
387 17 Noll, K. E. *et al.* Complex Genetic Architecture Underlies Regulation of Influenza-A-Virus-
388 Specific Antibody Responses in the Collaborative Cross. *Cell Rep* **31**, 107587,
389 doi:10.1016/j.celrep.2020.107587 (2020).
390 18 Price, A. *et al.* Transcriptional Correlates of Tolerance and Lethality in Mice Predict Ebola
391 Virus Disease Patient Outcomes. *Cell Rep* **30**, 1702-1713 e1706,
392 doi:10.1016/j.celrep.2020.01.026 (2020).
393 19 Sarkar, S. & Heise, M. T. Mouse Models as Resources for Studying Infectious Diseases.
394 *Clin Ther* **41**, 1912-1922, doi:10.1016/j.clinthera.2019.08.010 (2019).
395 20 Roberts, A., Pardo-Manuel de Villena, F., Wang, W., McMillan, L. & Threadgill, D. W. The
396 polymorphism architecture of mouse genetic resources elucidated using genome-wide
397 resequencing data: implications for QTL discovery and systems genetics. *Mamm*
398 *Genome* **18**, 473-481, doi:10.1007/s00335-007-9045-1 (2007).
399 21 Srivastava, A. *et al.* Genomes of the Mouse Collaborative Cross. *Genetics* **206**, 537-556,
400 doi:10.1534/genetics.116.198838 (2017).
401 22 Williamson, E. J. *et al.* Factors associated with COVID-19-related death using
402 OpenSAFELY. *Nature* **584**, 430-436, doi:10.1038/s41586-020-2521-4 (2020).
403 23 Ashbrook, D. G. *et al.* A platform for experimental precision medicine: The extended
404 BXD mouse family. *Cell Syst* **12**, 235-247 e239, doi:10.1016/j.cels.2020.12.002 (2021).
405 24 Gan, E. S. *et al.* A mouse model of lethal respiratory dysfunction for SARS-CoV-2
406 infection. *Antiviral Res* **193**, 105138, doi:10.1016/j.antiviral.2021.105138 (2021).
407 25 Kumari, P. *et al.* Neuroinvasion and Encephalitis Following Intranasal Inoculation of
408 SARS-CoV-2 in K18-hACE2 Mice. *Viruses* **13**, doi:10.3390/v13010132 (2021).
409 26 Oladunni, F. S. *et al.* Lethality of SARS-CoV-2 infection in K18 human angiotensin-
410 converting enzyme 2 transgenic mice. *Nat Commun* **11**, 6122, doi:10.1038/s41467-020-
411 19891-7 (2020).
412 27 Francis, M. E. *et al.* SARS-CoV-2 infection in the Syrian hamster model causes
413 inflammation as well as type I interferon dysregulation in both respiratory and non-
414 respiratory tissues including the heart and kidney. *PLoS Pathog* **17**, e1009705,
415 doi:10.1371/journal.ppat.1009705 (2021).

416 28 Imai, M. *et al.* Syrian hamsters as a small animal model for SARS-CoV-2 infection and
417 countermeasure development. *Proc Natl Acad Sci U S A* **117**, 16587-16595,
418 doi:10.1073/pnas.2009799117 (2020).
419 29 Tostanoski, L. H. *et al.* Ad26 vaccine protects against SARS-CoV-2 severe clinical disease
420 in hamsters. *Nat Med* **26**, 1694-1700, doi:10.1038/s41591-020-1070-6 (2020).
421 30 Bernardes, J. P. *et al.* Longitudinal Multi-omics Analyses Identify Responses of
422 Megakaryocytes, Erythroid Cells, and Plasmablasts as Hallmarks of Severe COVID-19.
423 *Immunity* **53**, 1296-1314 e1299, doi:10.1016/j.immuni.2020.11.017 (2020).
424 31 Schulte-Schrepping, J. *et al.* Severe COVID-19 Is Marked by a Dysregulated Myeloid Cell
425 Compartment. *Cell* **182**, 1419-1440 e1423, doi:10.1016/j.cell.2020.08.001 (2020).
426 32 Schultze, J. L. & Aschenbrenner, A. C. COVID-19 and the human innate immune system.
427 *Cell* **184**, 1671-1692, doi:10.1016/j.cell.2021.02.029 (2021).
428 33 Arunachalam, P. S. *et al.* Systems biological assessment of immunity to mild versus
429 severe COVID-19 infection in humans. *Science* **369**, 1210-1220,
430 doi:10.1126/science.abc6261 (2020).
431 34 Bastard, P. *et al.* Autoantibodies against type I IFNs in patients with life-threatening
432 COVID-19. *Science* **370**, doi:10.1126/science.abd4585 (2020).
433 35 Bost, P. *et al.* Host-Viral Infection Maps Reveal Signatures of Severe COVID-19 Patients.
434 *Cell* **181**, 1475-1488 e1412, doi:10.1016/j.cell.2020.05.006 (2020).
435 36 Chakraborty, S. *et al.* Proinflammatory IgG Fc structures in patients with severe COVID-
436 19. *Nat Immunol* **22**, 67-73, doi:10.1038/s41590-020-00828-7 (2021).
437 37 Consiglio, C. R. *et al.* The Immunology of Multisystem Inflammatory Syndrome in
438 Children with COVID-19. *Cell* **183**, 968-981 e967, doi:10.1016/j.cell.2020.09.016 (2020).
439 38 Mathew, D. *et al.* Deep immune profiling of COVID-19 patients reveals distinct
440 immunotypes with therapeutic implications. *Science* **369**, doi:10.1126/science.abc8511
441 (2020).
442 39 Shen, B. *et al.* Proteomic and Metabolomic Characterization of COVID-19 Patient Sera.
443 *Cell* **182**, 59-72 e15, doi:10.1016/j.cell.2020.05.032 (2020).
444 40 Silvin, A. *et al.* Elevated Calprotectin and Abnormal Myeloid Cell Subsets Discriminate
445 Severe from Mild COVID-19. *Cell* **182**, 1401-1418 e1418, doi:10.1016/j.cell.2020.08.002
446 (2020).
447 41 Takahashi, T. *et al.* Sex differences in immune responses that underlie COVID-19 disease
448 outcomes. *Nature* **588**, 315-320, doi:10.1038/s41586-020-2700-3 (2020).
449 42 Wilk, A. J. *et al.* A single-cell atlas of the peripheral immune response in patients with
450 severe COVID-19. *Nat Med* **26**, 1070-1076, doi:10.1038/s41591-020-0944-y (2020).
451 43 Lucas, C. *et al.* Longitudinal analyses reveal immunological misfiring in severe COVID-19.
452 *Nature* **584**, 463-469, doi:10.1038/s41586-020-2588-y (2020).
453 44 Zhang, Q. *et al.* Inborn errors of type I IFN immunity in patients with life-threatening
454 COVID-19. *Science* **370**, doi:10.1126/science.abd4570 (2020).
455 45 Blanco-Melo, D. *et al.* Imbalanced Host Response to SARS-CoV-2 Drives Development of
456 COVID-19. *Cell* **181**, 1036-1045 e1039, doi:10.1016/j.cell.2020.04.026 (2020).
457 46 Ziegler, C. G. K. *et al.* Impaired local intrinsic immunity to SARS-CoV-2 infection in severe
458 COVID-19. *Cell* **184**, 4713-4733 e4722, doi:10.1016/j.cell.2021.07.023 (2021).

459 47 Zanoni, I. Interfering with SARS-CoV-2: are interferons friends or foes in COVID-19? *Curr*
460 *Opin Virol* **50**, 119-127, doi:10.1016/j.coviro.2021.08.004 (2021).
461 48 Delorey, T. M. *et al.* COVID-19 tissue atlases reveal SARS-CoV-2 pathology and cellular
462 targets. *Nature* **595**, 107-113, doi:10.1038/s41586-021-03570-8 (2021).
463

464 **Table 1:** Summary of percent survival, weight loss, virus burden and BAL cytokine profiles in

465 K18-hACE2 x CC Founder F1 progeny.

				Peak weight loss		Average Virus Titers in Lung		IFNα in BAL	Cytokine profile BAL	
Strain	Sex	%Survival	Mean time to death (days)	%	DPI	3 dpi Mean (Std Dev)	6 dpi Mean (Std Dev)	3dpi	3 dpi	6 dpi
K18-hACE2	M	14	6	16.7	7	1.5e6 (1.9e6)	7.6e4 (1.3e5)	Low	No/Low	High Group A and Group B
	F	29	7	12.0	7	1.5e6 (1.4e6)	8.2e3 (5.7e3)	Low		
A/J x K18-hACE2 F1	M	33	8	15.0	7	2.8e6 (2.2e6)	4.65e4 (6.9e4)	Low	No/Low	High Group A and Group B
	F	66	UD	6.1	7	3.3e6 (2.4e6)	3.0e4 (2.9e4)	Low		
PWK x K18-hACE2 F1	M	83	UD	-	-	1.6e5 (2.3e5)	BLD	High	High Group A	Moderate Group A and Group B
	F	83	UD	7.0	7	1.5e4 (2.3e4)	BLD	Low		
NZO x K18-hACE2 F1	M	86	UD	13.9	9	2.6e6 (2.9e6)	3.8e3 (3.7e3)	High	High Group A	High Group A and B
	F	71	UD	21.9	9	2.0e6 (9.4e5)	1.3e3 (1.0e3)	High		
129S1J x K18-ACE2 F1	M	86	UD	11.8	7	1.1e6 (8.3e5)	3.0e3 (2.8e3)	High	High Group A	High Group A and Group B
	F	71	UD	12.0	7	8.1e5 (6.4e4)	2.4e4 (4.0e4)	Moderate		
CAST x K18-ACE2 F1	M	0	6	17.2	7	3.4e6 (3.2e6)	4.8e5(3.7e5)	Low	Low Group A	Low Group A Males = Females
	F	50	15.5	35.8	8	1.75e6(1.5e6)	3.4e4 (2.9e4)	Low		
NOD x K18-ACE2 F1	M	33	6.5	6.0	6	1.7e6 (3.7e6)	4.8e3 (5.3e3)	Low	No/Low	Group A and Group B Males > Females
	F	83	UD	-	-	4.3e5 (7.4e5)	6.4e3 (8.1e3)	Low		
WSB x K18-ACE2 F1	M	66	UD	32.0	11	4.2e6 (1.8e6)	3.1e4 (1.6e4)	High	Moderate Group A	Group A and B Males > Females
	F	0	8	25.1	8	3.7e6 (4.1e6)	2.5e4 (1.2e4)	High		
BALB/c x K18-ACE2 F1	M	100	UD	3.0	5	6.0e5 (5.5e5)	1.6e4 (1.3e4)	Moderate	No/Low	Group A and B Females > Males
	F	66	UD	8.3	6	4.4e5 (4.3e5)	6.0e2 (1.2e3)	High	High Group A	
DBA/2 x K18-ACE2 F1	M	57	UD	16.0	10	1.5e6 (1.7e6)	1.7e4 (2.2e4)	Moderate	No/Low	Group A and B Females > Males
	F	71	UD	3.6	6	2.0e6 (1.0e6)	1.2e3 (1.0e3)	Moderate		

466 UD: undetermined

467 BLD: below limit of detection

468

469

a Sensitive

C57Bl/6JxK18-hACE2

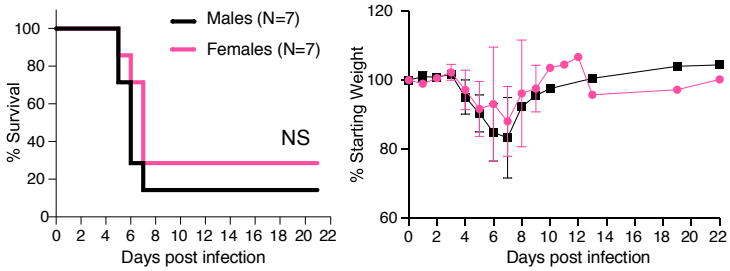

A/JxK18-hACE2

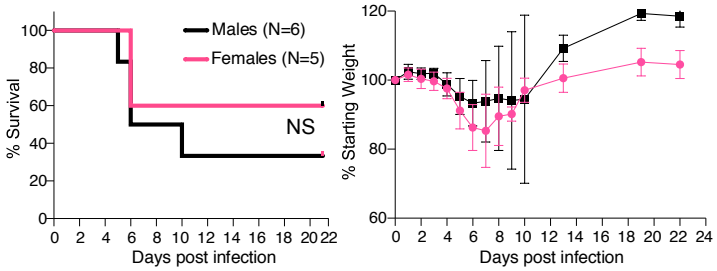

b Resistant

PWKxK18-hACE2

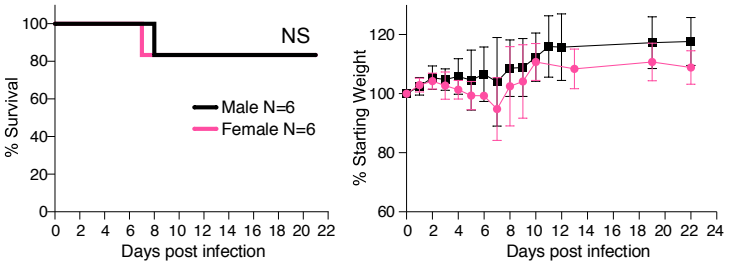

NZOxK18-hACE2

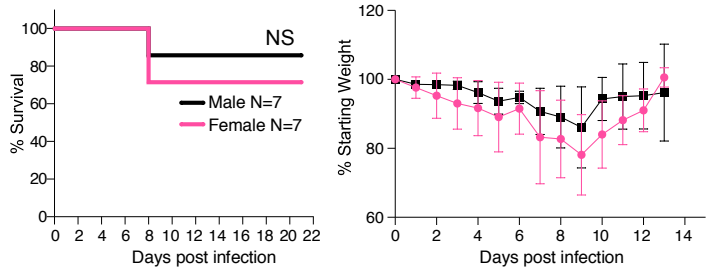

129S1xK18-hACE2

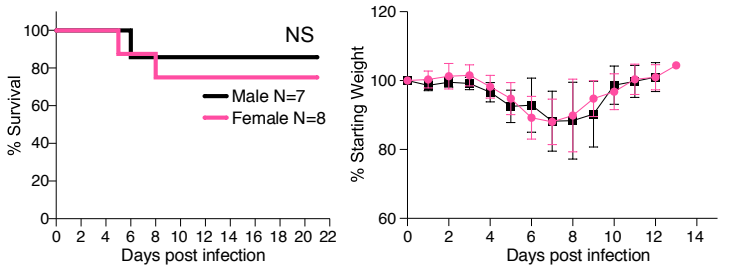

c Sensitive with Sex Bias

CASTxK18-hACE2

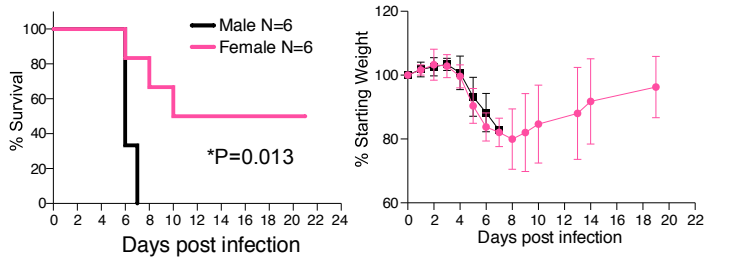

NODxK18-hACE2

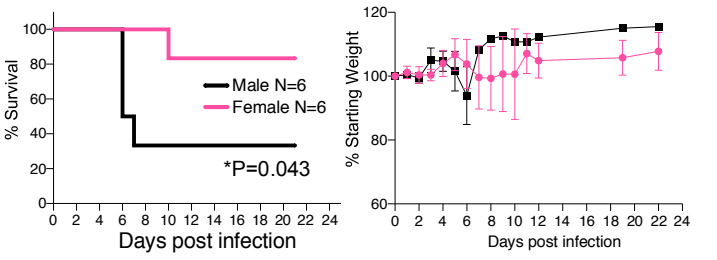

WSBxK18-hACE2

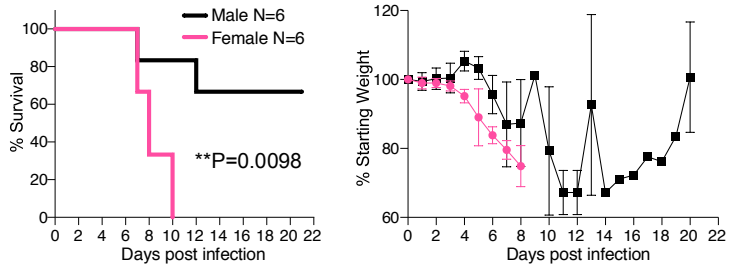

Fig. 1

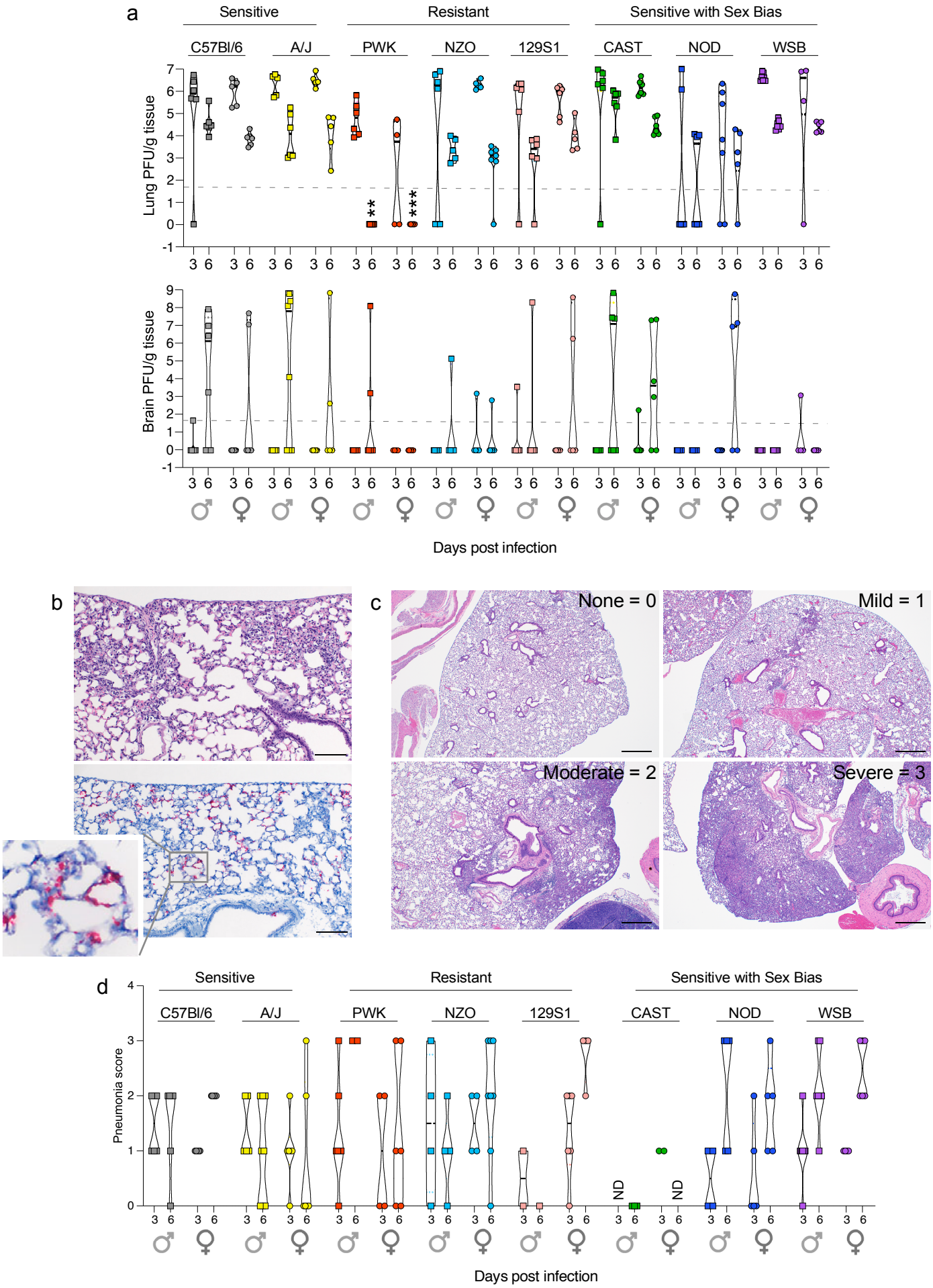
a
Sensitive
Resistant
Sensitive with Sex Bias
C57Bl/6
A/J
PWK
NZO
129S1
CAST
NOD
WSB
Lung PFU/g tissue
Brain PFU/g tissue
Days post infection
b
c
None = 0
Mild = 1
Moderate = 2
Severe = 3
d
Pneumonia score
ND
Days post infection

Figure 2

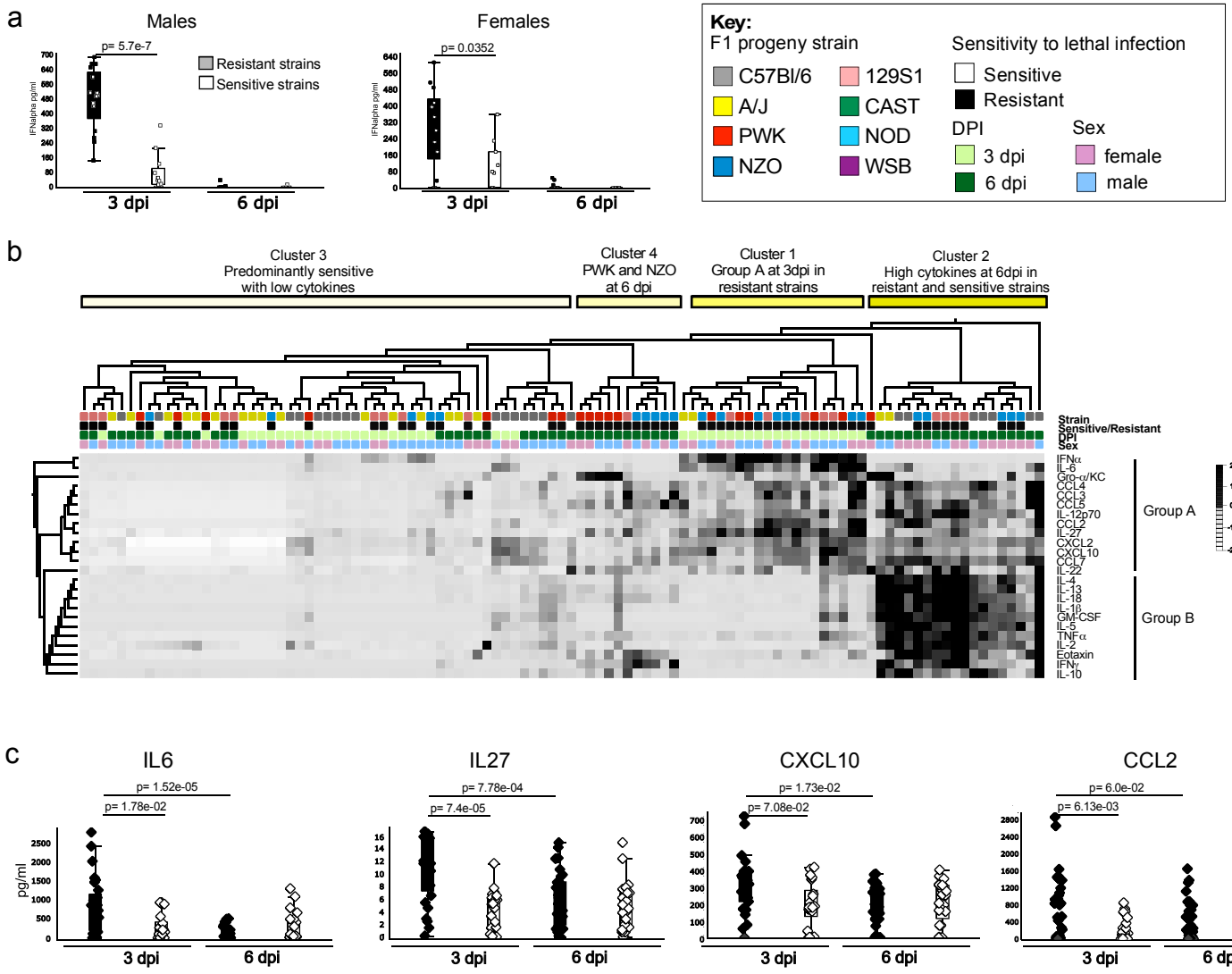
a
Males
Females
p= 5.7e-7
p= 0.0352
Resistant strains
Sensitive strains
IFNalpha pg/ml
3 dpi
6 dpi
Key:
F1 progeny strain
C57Bl/6
129S1
A/J
CAST
PWK
NOD
NZO
WSB
Sensitivity to lethal infection
Sensitive
Resistant
DPI
3 dpi
6 dpi
Sex
female
male
b
Cluster 3
Predominantly sensitive
with low cytokines
Cluster 4
PWK and NZO
at 6 dpi
Cluster 1
Group A at 3dpi in
resistant strains
Cluster 2
High cytokines at 6dpi in
reistant and sensitive strains
Strain
Sensitive/Resistant
DPI
Sex
IFNα
IL-6
Gro-α/KC
CCL4
CCL3
CCL5
IL-12p70
CCL2
IL-27
CXCL2
CXCL10
CCL7
IL-22
IL-4
IL-13
IL-18
IL-1β
GM-CSF
IL-5
TNFα
IL-2
Eotaxin
IFNγ
IL-10
Group A
Group B
c
IL6
IL27
CXCL10
CCL2
p= 1.52e-05
p= 1.78e-02
p= 7.78e-04
p= 7.4e-05
p= 1.73e-02
p= 7.08e-02
p= 6.0e-02
p= 6.13e-03
pg/ml
3 dpi
6 dpi

Figure 3

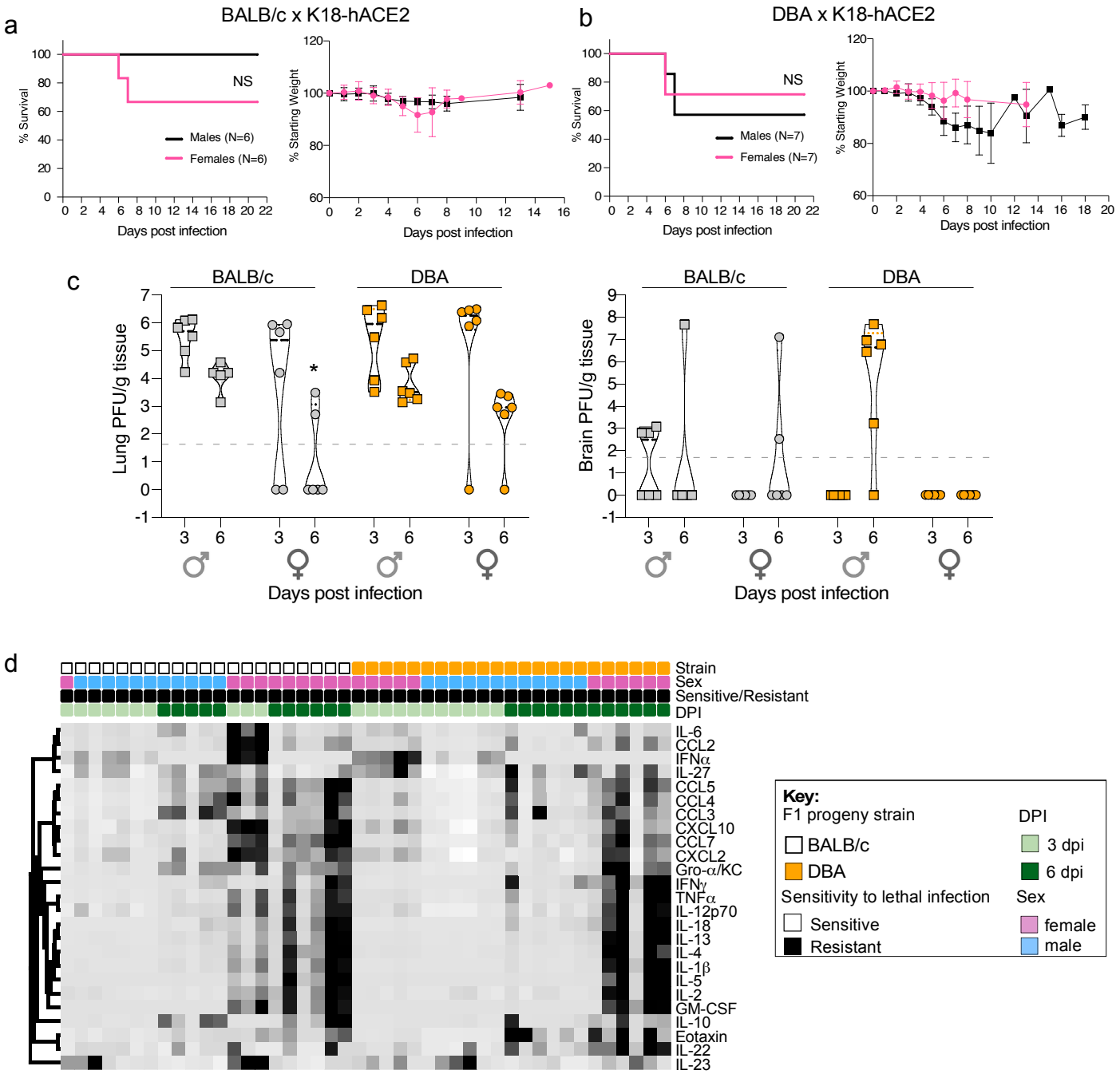
a
BALB/c x K18-hACE2
% Survival
NS
Males (N=6)
Females (N=6)
Days post infection
% Starting Weight
Days post infection
b
DBA x K18-hACE2
% Survival
NS
Males (N=7)
Females (N=7)
Days post infection
% Starting Weight
Days post infection
c
BALB/c
DBA
Lung PFU/g tissue
Days post infection
BALB/c
DBA
Brain PFU/g tissue
Days post infection
d
Strain
Sex
Sensitive/Resistant
DPI
IL-6
CCL2
IFNα
IL-27
CCL5
CCL4
CCL3
CXCL10
CCL7
CXCL2
Gro-α/KC
IFNγ
TNFα
IL-12p70
IL-18
IL-13
IL-4
IL-1β
IL-5
IL-2
GM-CSF
IL-10
Eotaxin
IL-22
IL-23
Key:
F1 progeny strain
BALB/c
DBA
Sensitivity to lethal infection
Sensitive
Resistant
DPI
3 dpi
6 dpi
Sex
female
male

Fig. S1

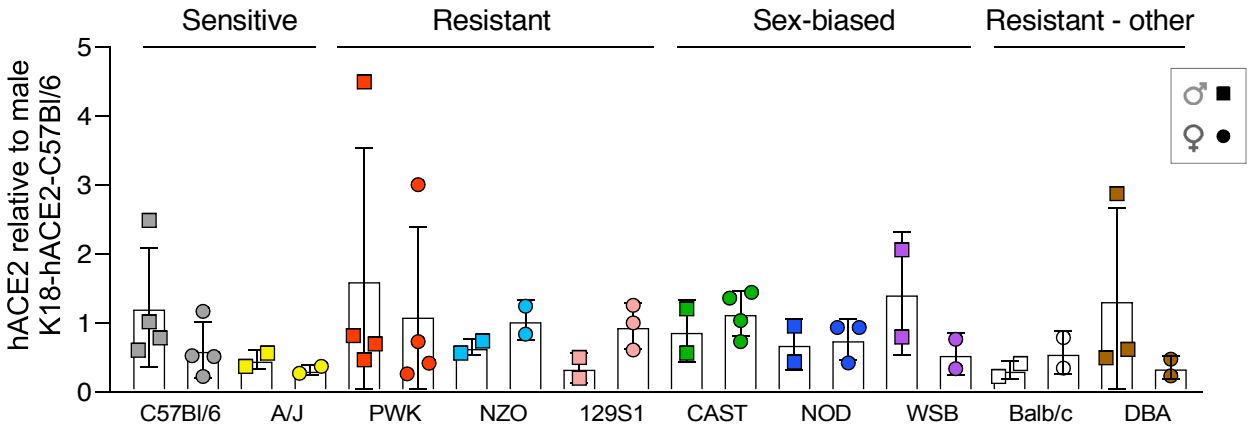
Sensitive
Resistant
Sex-biased
Resistant - other
hACE2 relative to male
K18-hACE2-C57Bl/6
5
4
3
2
1
0
C57Bl/6
A/J
PWK
NZO
129S1
CAST
NOD
WSB
Balb/c
DBA
♂
♀

Fig. S2

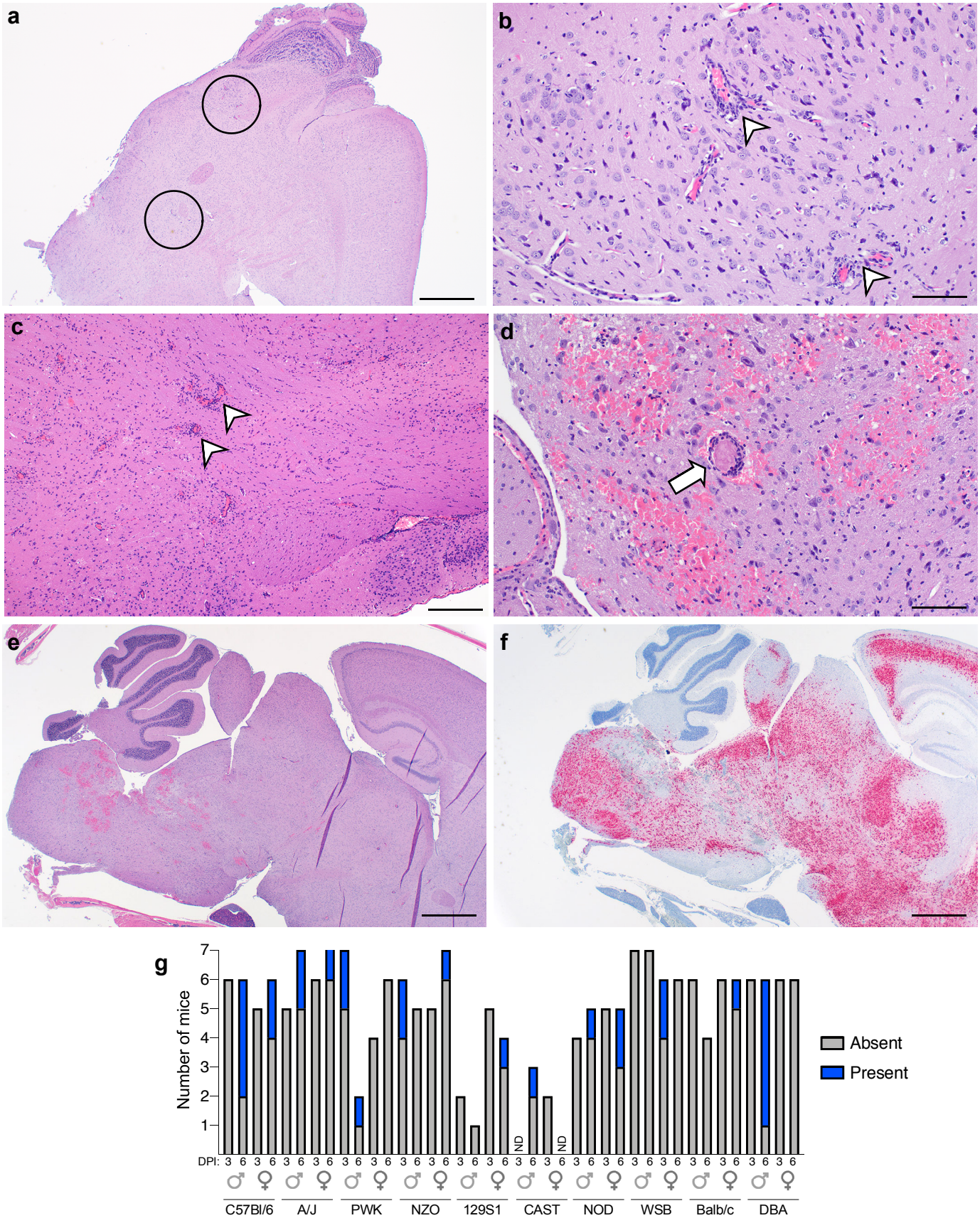
a
b
c
d
e
f
g
Number of mice
7
6
5
4
3
2
1
DPI: 3 6 3 6 3 6 3 6 3 6 3 6 3 6 3 6 3 6 3 6 3 6 3 6 3 6 3 6 3 6 3 6 3 6 3 6 3 6 3 6 3 6
ND
ND
♂ ♀ ♂ ♀ ♂ ♀ ♂ ♀ ♂ ♀ ♂ ♀ ♂ ♀ ♂ ♀ ♂ ♀ ♂ ♀
C57Bl/6
A/J
PWK
NZO
129S1
CAST
NOD
WSB
Balb/c
DBA
Absent
Present

Fig. S3

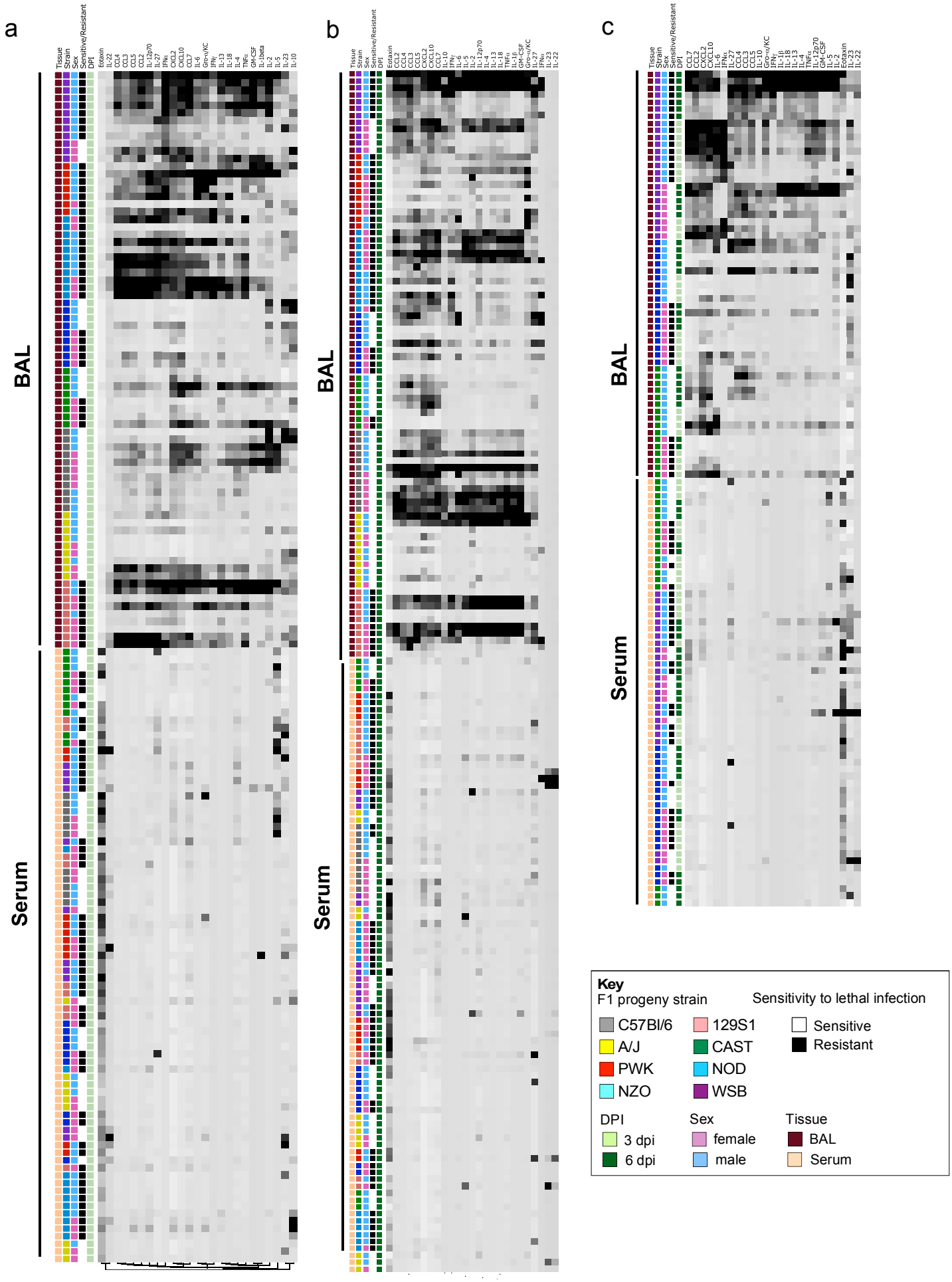
a
b
c
BAL
Serum
Tissue
Strain
Sex
Sensitive/Resistant
DPI
Key
F1 progeny strain
C57Bl/6
A/J
PWK
NZO
129S1
CAST
NOD
WSB
Sensitivity to lethal infection
Sensitive
Resistant
DPI
3 dpi
6 dpi
Sex
female
male
Tissue
BAL
Serum

Fig. S4

Male BAL cytokine panel

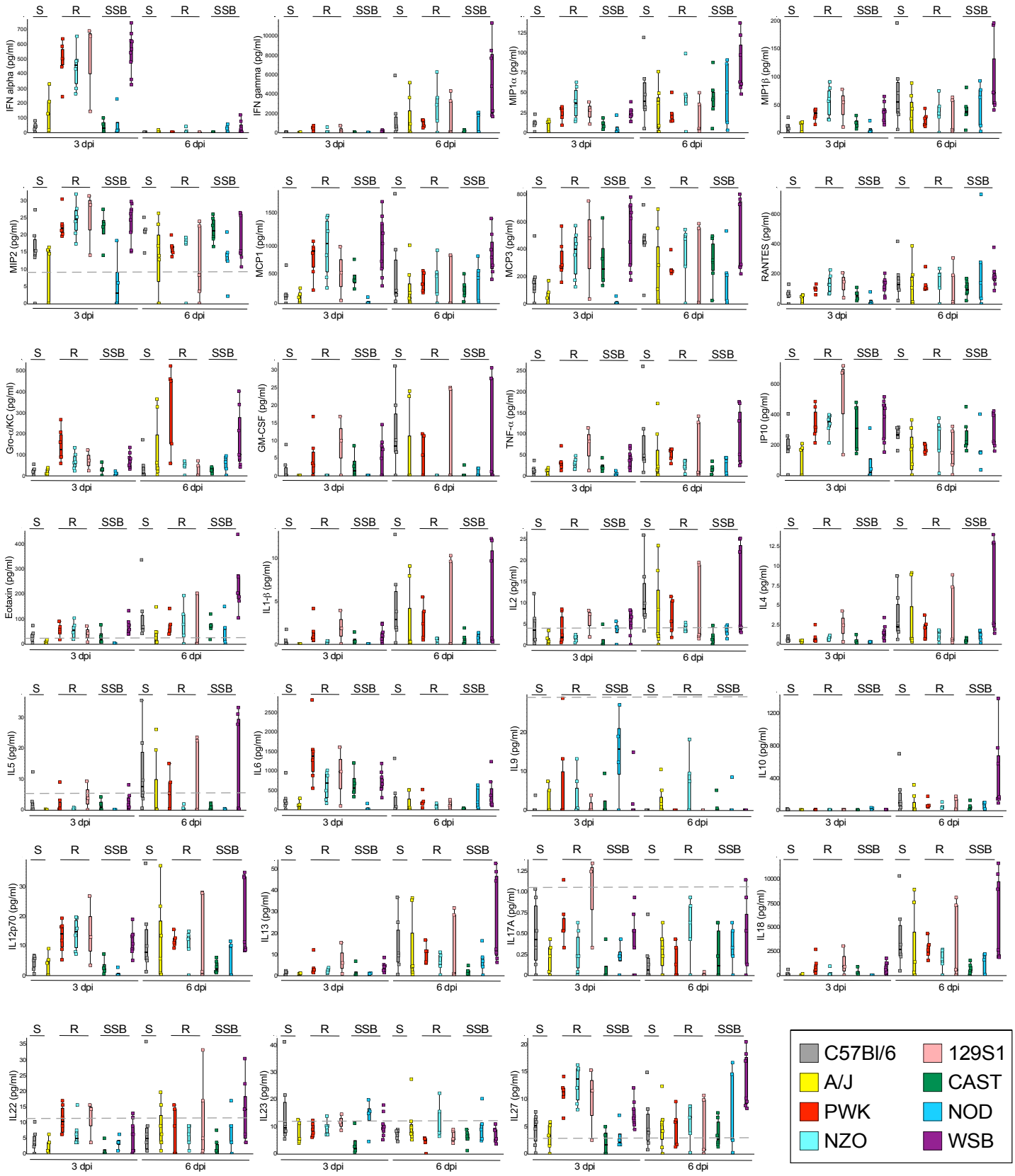

Fig. S5

Male serum cytokine panel

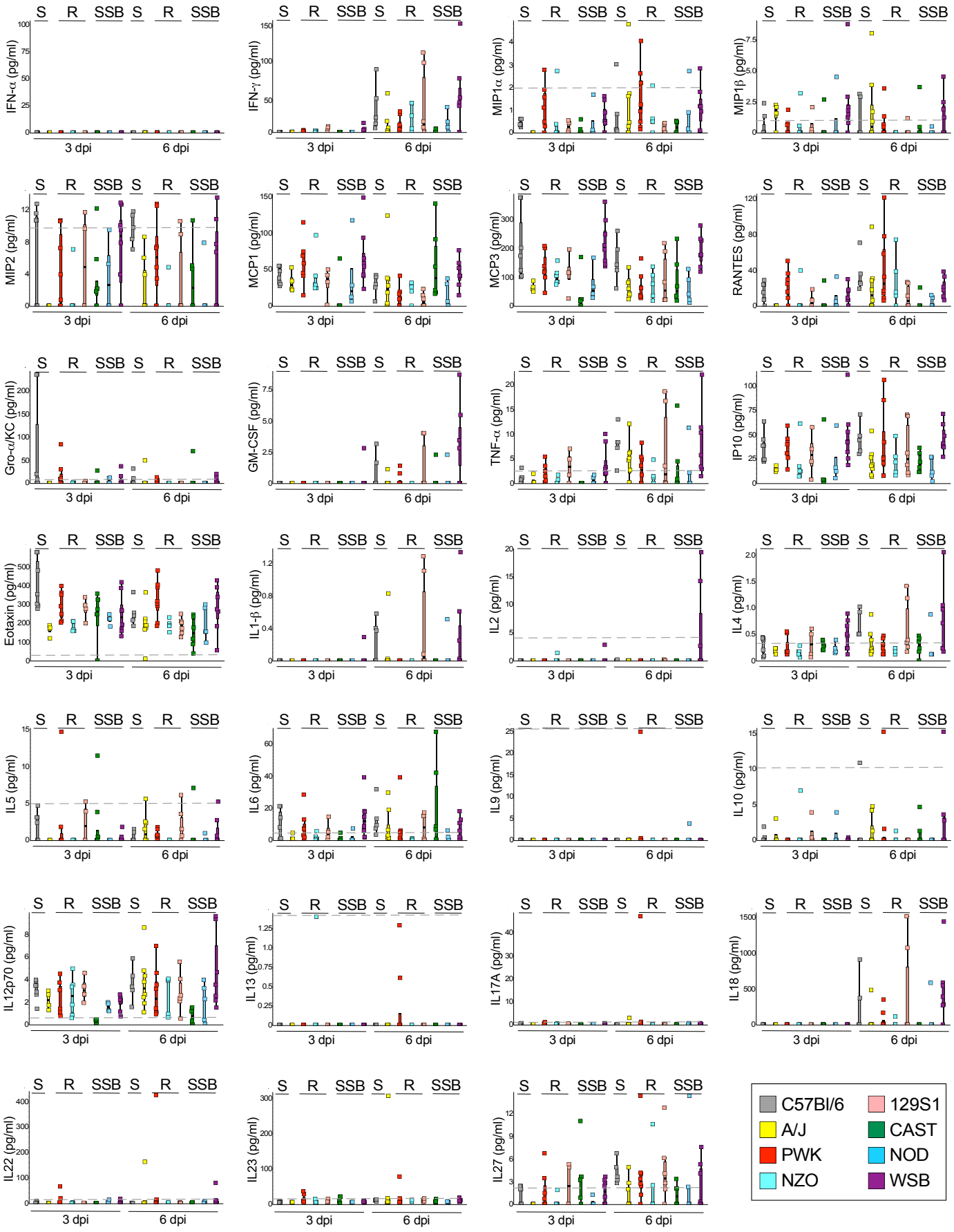

Fig. S6

Female BAL cytokine panel

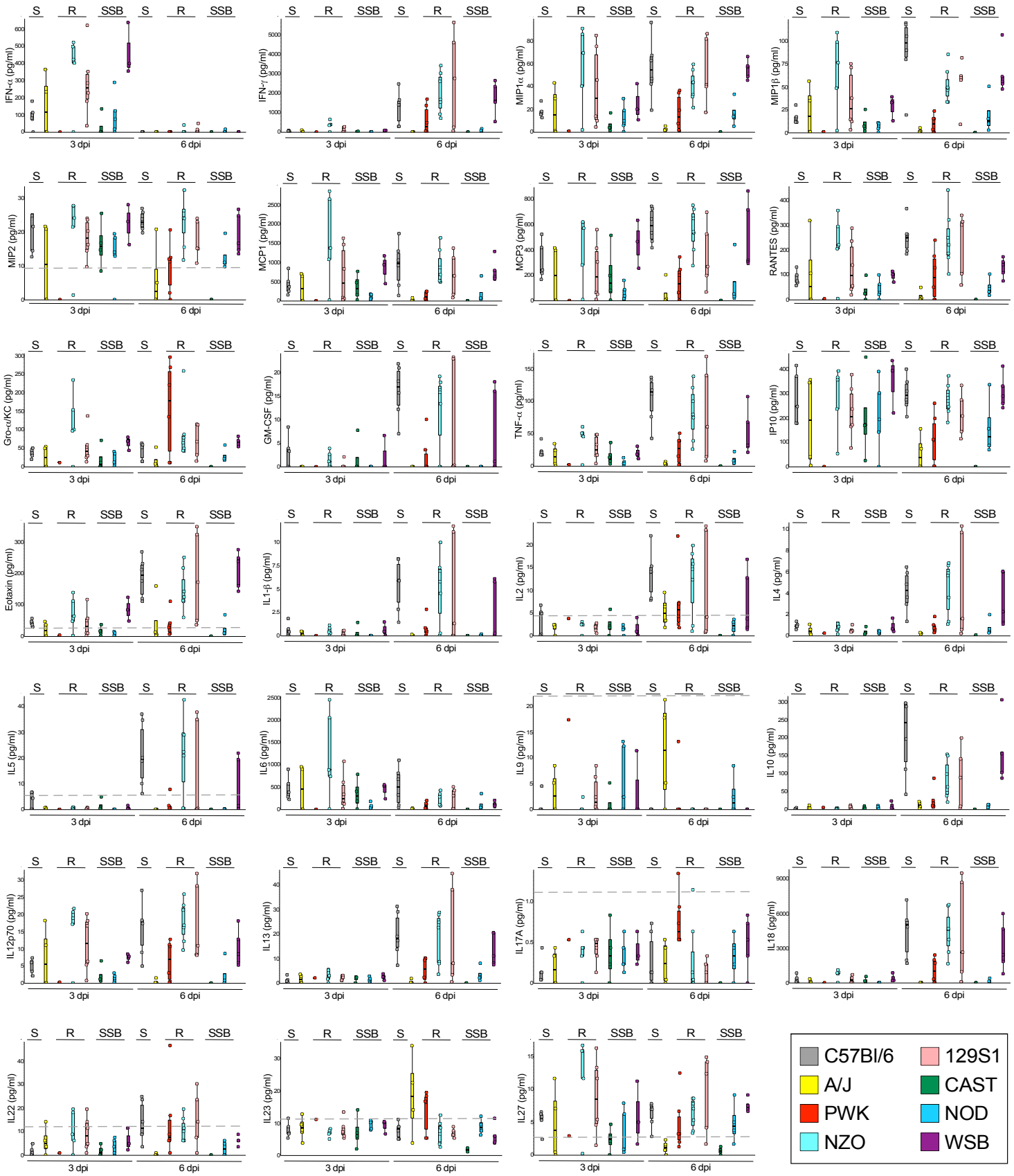

Fig. S7

Female serum cytokine panel

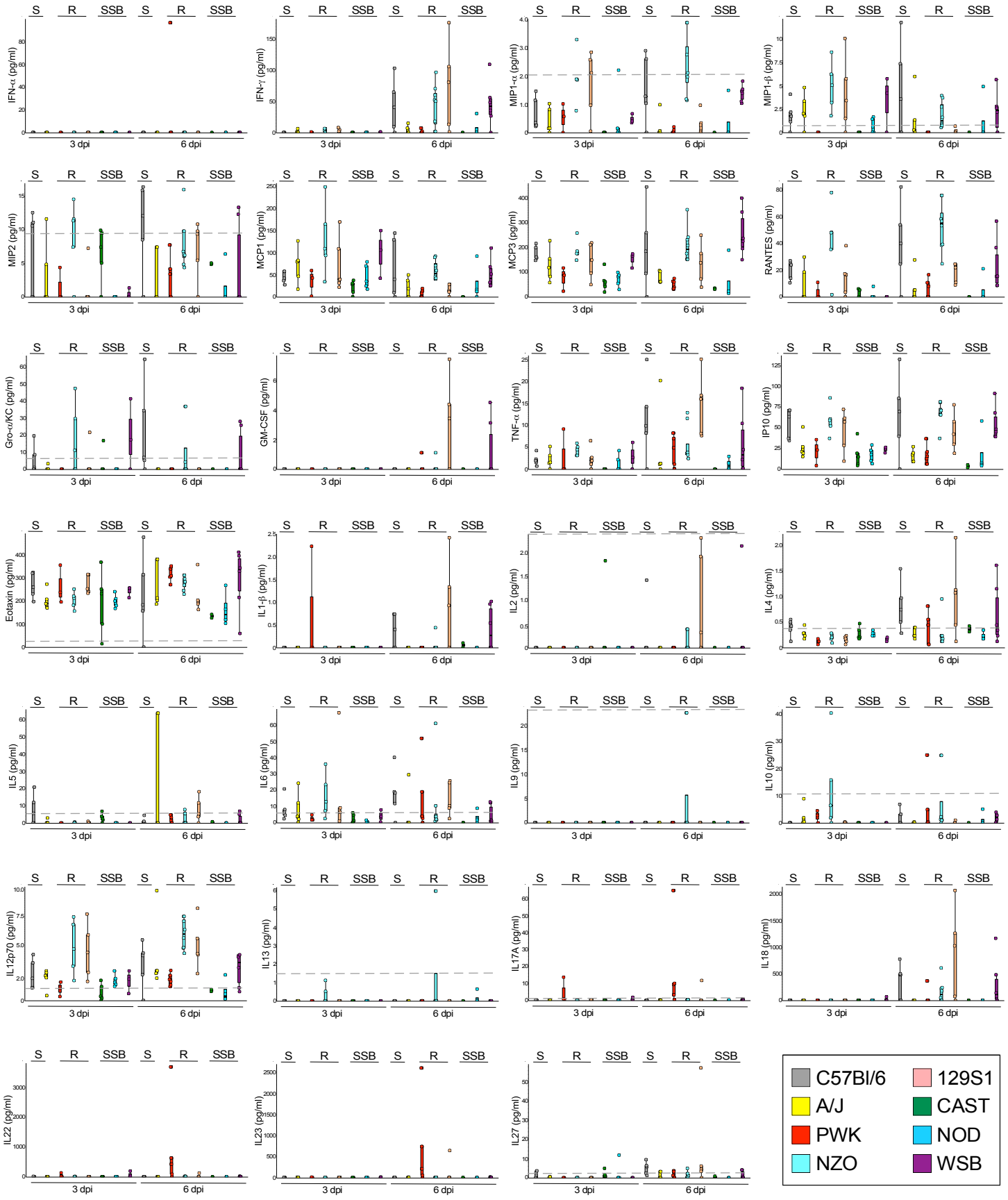

Fig. S8